Factors Driving Past Trends in Arctic Precipitation and Their Future Changes

Seiji Yukimoto[1], Naga Oshima[2], Hideaki Kawai[2], Makoto Deushi[2], and Takuro Aizawa[3]

[1]Meteorological Research Institute
[2]Meteorological Research Institute
[3]National Institute of Polar Research

December 3, 2023

Abstract

The Arctic is notable as a region where the greatest rate of increase in precipitation associated with global warming is anticipated. The Arctic precipitation simulated by the Coupled Model Intercomparison Project phase 6 multimodels showed a strong increasing trend in the recent past since the 1980s as a result of the continued strengthening of greenhouse gas forcing. Meanwhile, the suppression by aerosol forcing, which dominated in earlier periods, has been leveled off. From an energetic perspective, the constraining factors of increased atmospheric radiative cooling and reduced heat transport from lower latitudes contributed equally to the recent increase in Arctic precipitation. Future Arctic precipitation will change in proportion to the temperature change, but the fractional contributions of the constraining factors will remain stable across various scenarios. The implications for the doubling of the Arctic amplification factor of precipitation changes relative to that of temperature changes are also discussed.

Hosted file

980263_0_art_file_11618764_s4v2yh.docx available at https://authorea.com/users/533526/articles/690152-factors-driving-past-trends-in-arctic-precipitation-and-their-future-changes

AGU PUBLICATIONS

Factors Driving Past Trends in Arctic Precipitation and Their Future Changes

S. Yukimoto[1], N. Oshima[1], H. Kawai[1], M. Deushi[1], and T. Aizawa[1,2]

[1] Meteorological Research Institute, Japan Meteorological Agency, Tsukuba, Japan

[2] National Institute of Polar Research, Tachikawa, Japan

Corresponding author: Seiji Yukimoto (yukimoto@mri-jma.go.jp)

Key Points:

- The rapid increase in Arctic precipitation in the recent past is examined from multimodel simulations.
- The rapid increase is driven by accelerating greenhouse gas concentrations and plateauing growth in anthropogenic aerosol emissions.
- Increased radiative cooling and reduced poleward heat transport equally constrained the Arctic precipitation changes.

Abstract

The Arctic is notable as a region where the greatest rate of increase in precipitation associated with global warming is anticipated. The Arctic precipitation simulated by the Coupled Model Intercomparison Project phase 6 multimodels showed a strong increasing trend in the recent past since the 1980s as a result of the continued strengthening of greenhouse gas forcing. Meanwhile, the suppression by aerosol forcing, which dominated in earlier periods, has been leveled off. From an energetic perspective, the constraining factors of increased atmospheric radiative cooling and reduced heat transport from lower latitudes contributed equally to the recent increase in Arctic precipitation. Future Arctic precipitation will change in proportion to the temperature change, but the fractional contributions of the constraining factors will remain stable across various scenarios. The implications for the doubling of the Arctic amplification factor of precipitation changes relative to that of temperature changes are also discussed.

Plain Language Summary

The Arctic region is inherently a low-precipitation area. However, because of global warming, precipitation is expected to significantly increase in the Arctic region compared with the global average when viewed as a percentage change from the original precipitation. This severely affects climate change in the Arctic environment. The latest climate model simulations show that there has been a rapid increase in precipitation in the Arctic region in the recent past. The driving factors behind the rapid increase are the effects of the accelerating growth of greenhouse gas concentrations, which were previously suppressed by the increasing anthropogenic aerosol emissions before the 1980s. Based on the heat budget of the atmosphere, we identified important factors contributing to these precipitation changes. These include enhanced radiative cooling (responding locally to increased air temperature) and reduced heat transport from lower latitudes due to greater temperature increases at higher latitudes. Future precipitation will change in proportion to the temperature change while maintaining consistent fractional contributions across different scenarios.

1 Introduction

Understanding the factors of past changes in the Arctic mean precipitation is important for future projections of climate change in the Arctic region. Associated with global warming, the temperature increase in the Arctic region is known to be larger than those in lower latitudes (Manabe and Wetherald, 1975; Holland and Bitz, 2003; Pithan and Mauritsen, 2014; Previdi et al., 2021), the so-called Arctic amplification. Precipitation is also expected to increase at a greater rate in the Arctic region (Bengtsson et al., 2011; Bintanja and Selten, 2014; McCrystall et al., 2021), which means that the relative increase in precipitation is greater in the Arctic region, where precipitation is inherently low.

Many previous studies have discussed the causes of precipitation increase in the Arctic mainly in terms of the moisture budget, such as increased moisture transport from lower latitudes (Bengtsson et al., 2011; Bintanja et al., 2020) and increased evaporation due to sea ice loss (Bintanja and Selten, 2014). Meanwhile, the global mean precipitation change is constrained by the radiative cooling rate of the atmosphere (Allen and Ingram, 2002; Pendergrass and Hartmann, 2014), not the rate of water vapor increase, from the perspective of energetics. Such energetic constraints have also been applied to studies on regional precipitation changes (Muller and O'Gorman, 2011).

Recently, the factors that alter the Arctic hydrological cycle have also been discussed from the perspective of energetics (Pithan and Jung, 2021; Bonan et al., 2023), suggesting that changes in the radiative cooling of the atmosphere are essential factors in the “Arctic amplification” of precipitation changes. However, the drivers of past changes in Arctic precipitation remain unclear. The challenge is to determine how forcing factors, such as anthropogenic greenhouse gases (GHGs) and aerosols, alter constraining factors, such as radiative cooling and energy transport. The Arctic amplification of temperature changes exhibits similarity despite different forcing factors (Stjern et al., 2019). However, the Arctic amplification of precipitation changes is yet to be explored. Moreover, the trends in those factors must be understood for future applications.

In this paper, we analyzed the sixth phase of the Coupled Model Intercomparison Project (CMIP6) multimodel experiments to explore the contribution of each factor to past and future multidecadal trends in annual mean precipitation over the Arctic region. The Arctic amplification of precipitation changes is also interpreted.

2 Data and Methods

To investigate the drivers of past changes in precipitation, we analyzed multimodel data from the Detection and Attribution Model Intercomparison Project (DAMIP; Gillett et al., 2016) historical experiments with individual forcing: the anthropogenic aerosol forcing experiment (hist-aer), the well-mixed GHG forcing experiment (hist-GHG), and the natural (solar and volcanic activities) forcing experiment (hist-nat), in addition to the CMIP6 historical experiment (historical). To examine future changes in precipitation, we also analyzed multimodel data from five representative scenario experiments for shared socioeconomic pathways (ssp119, ssp126, ssp245, ssp370, and ssp585) in ScenarioMIP (O'Neill et al., 2016). We used data from all models (Table S1) for which the required variables were available, and three or more member runs were submitted. For each model, we made an ensemble average of all the runs submitted and then averaged those ensembles into a multimodel mean by averaging the ensembles with equal weights for each model.

If we ignore changes in the atmospheric heat storage because we are dealing with long-term changes, the column-integrated dry static energy (DSE) balance of the atmosphere can be expressed as

$$LP = -R + \nabla_{\mathrm{H}} S - F_{\mathrm{SH}} \quad (1)$$

(Muller and O'Gorman, 2011; Dagan & Stier, 2020; Yukimoto et al., 2022), where L is the latent heat of evaporation (2.5×10^6 J/kg), P is precipitation (kg/m^2/s), $\nabla_{\mathrm{H}} S$ is the horizontal divergence of the column-integrated DSE (W/m^2), and F_{SH} is the surface sensible heat flux (W/m^2, upward positive). The total DSE divergence ∇S can be expressed as $\nabla S = \nabla_{\mathrm{H}} S - F_{\mathrm{SH}}$; that is, the downward surface sensible heat flux corresponds to the DSE vertical divergence. $-R$ is the radiative cooling of the atmosphere, determined from the difference between the radiative budget at the top of the atmosphere and the surface. Long-term (30 years) linear trends were calculated for each term in equation (1) for each latitudinal zone for the historical periods (Period I: 1951–1980; Period II: 1981–2010), near future (Period III: 2016–2045), medium term (Period IV: 2046–2075), and the end of the 21st century (Period V: 2071–2100). The 60°N–90°N area average was defined as the Arctic mean.

To compare historical changes in simulated temperature and precipitation in the Arctic, we used HadCRUT5 (Morice et al., 2021) for temperature and GPCP-SG v2.3 (Adler et al., 2017) for precipitation as observations. Notably, however, satellite observations were not calibrated well because there were only a few long-term rain gauge precipitation observations in the polar regions and satellite retrievals were difficult because the ground surface was often covered with snow and ice. Surface air temperature and precipitation from the fifth-generation ECMWF atmospheric reanalysis (ERA5; Hersbach et al., 2020) were also used for comparison. For the reanalysis, precipitation was not directly assimilated except for some recent radar data.

3 Results and Discussion

3.1 Historical Changes in Temperature and Precipitation in the Arctic

The CMIP6 multimodel mean well reproduced the observed historical changes in temperature for the Arctic region and the global mean (Figure 1a). Arctic air temperatures have been rising rapidly since the 1980s. The rate of temperature increase was much greater than the global average, indicating a distinct Arctic amplification. The simulated precipitation changes were analogous to temperature changes (Figure 1b). Precipitation in the Arctic region has increased rapidly since the 1980s (Period II), and the rate of increase was much greater than the global average, indicating an Arctic amplification of precipitation changes. In an earlier period (Period I), precipitation showed a slight negative trend in both the global and Arctic regions.

Because the variation of the multimodel mean resulted from the averaging of many ensemble members, internal variability was mostly eliminated. In contrast, the observed GPCP precipitation and ERA5 reanalysis precipitation were difficult for statistically evaluating trends because of the large internal climate variability. In addition to the effects of internal variability, the GPCP and ERA5 trends were likely to have large uncertainties arising from the lack of observations. Nevertheless, the contrast between the global and Arctic mean trends in Period II appeared to be consistent with the model reproduction.

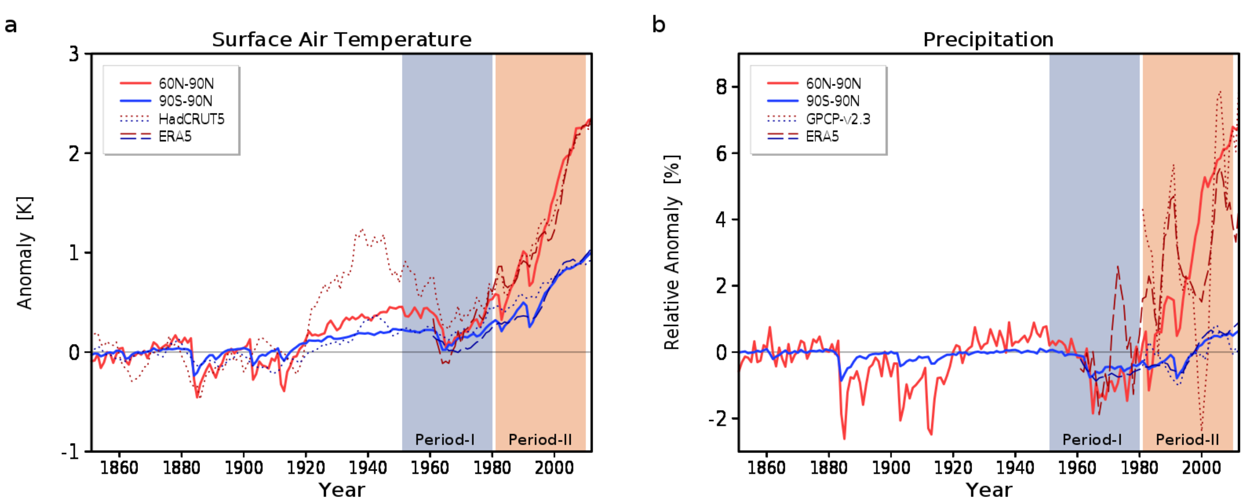

Figure 1. Time series of annual mean (a) surface air temperature and (b) precipitation anomalies for the Arctic (60°N–90°N) mean (red line) and global mean (blue line). Solid lines are anomalies from the 1851 to 1880 mean of the multimodel mean of the CMIP6 historical experiment. Relative anomalies (%) are shown for precipitation. Dotted lines in (a) and (b) indicate the observed surface air temperature HadCRUT5 and observed precipitation GPCP-SG

v2.3, respectively. The dashed lines indicate the observed surface air temperature and precipitation from the ERA5 reanalysis. The relative values of the observations and reanalysis are offset so that the 1981–2010 averages match.

3.2 Forcing Factors for Historical Precipitation Changes

The time series of Arctic mean precipitation for the experiments to separate the forcing factors are shown in Figure S1, where the GHG forcing response shows a consistent increase in temperature and precipitation over the entire historical period, with the rate of increase seemingly increasing around the 1970s. In contrast, the aerosol forcing response shows a significant decline in both temperature and precipitation from the 1950s until the 1970s, with the decline bottoming out after the 1980s. Because of this trend difference before and after 1980, we divided the period into Period I (1951–1980) and Period II (1981–2010) and analyzed the trend for each period.

Figure 2a shows the Arctic mean precipitation trend and its components broken down by forcing factor. During Period I, the dominant negative trend due to aerosol forcing was greatly mitigated by the positive trend due to GHG forcing, resulting in a weak negative historical trend. In Period II, whereas the aerosol forcing showed almost no trend, the GHG forcing was accelerated and became dominant, resulting in a large increasing trend in the historical precipitation. Such a contrast in the combined responses of aerosol and GHG forcing in the historical period has also been reported for temperature changes in the Arctic (England et al., 2021; Aizawa et al., 2022). The contribution of natural forcing was small in both periods.

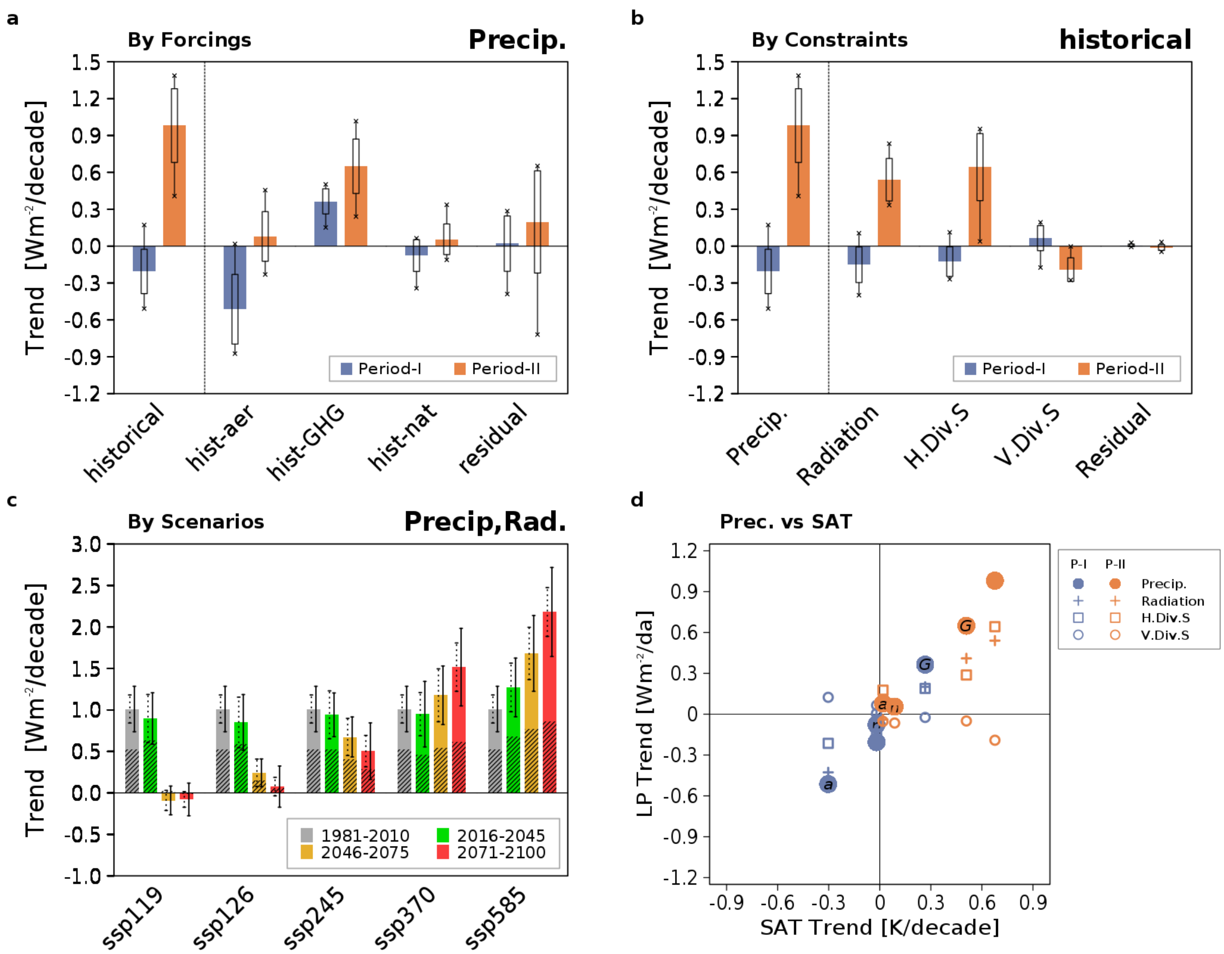

Figure 2. (a–c) Arctic mean precipitation trend and its breakdowns by forcing factors and constraining factors based on the historical, DAMIP, and ScenarioMIP experiments. (a) Decompositions of total forcing (historical) into aerosol forcing (hist-aer), GHG forcing (hist-GHG), natural forcing (hist-nat), and residual and (b) decompositions of precipitation trend in the historical into radiative cooling (Radiation), horizontal (H.Div.S) and vertical (V.Div.S) divergence of DSE, and residual (Residual) components for Periods I (blue) and II (orange), respectively. (c) Present and future trends of Arctic mean precipitation (the shaded part is the radiative cooling component, and the rest is mostly DSE horizontal divergence) based on the historical experiment for Period II (1981–2010, gray) and each scenario experiment in the ScenarioMIP experiments (ssp119, ssp126, ssp245, ssp370, and ssp585) for Periods III (2016–2045, green), IV (2046–2075, yellow), and V (2071–2100, red). Solid and dashed vertical lines indicate standard deviations of intermodel spread for the DSE divergence and radiative cooling components, respectively. (d) Scatterplot of the trend of Arctic precipitation and its constraining factor components against the Arctic temperature trend in the DAMIP multimodel mean. The type of mark indicates the constraining factor (as shown in the legend). The color indicates the period (blue: Period I; orange: Period II). Letters on the marks indicate the type of DAMIP experiment (no mark: historical; “a”: hist-aer; “G”: hist-GHG; “n”: hist-nat).

Examining the meridional distribution of trends in relative precipitation change by forcing factor (Figure 3) revealed that both the negative trend due to aerosol forcing (Period I) and the positive trend due to GHG forcing (Periods I and II) were larger at higher latitudes in the Northern Hemisphere (NH) extratropics. The offsetting of aerosol and GHG forcings in Period I and the dominance of GHG forcing in Period II was also seen in the Southern Hemisphere (SH) extratropics except for Antarctica. In the tropics, the north–south asymmetric trend in Period I with a decrease in NH and an increase in SH (Figure 3a) could be attributed to aerosol forcing (Figure S2a, b). The southward shift of the intertropical convergence zone reproduced by the CMIP6 models (Yukimoto et al., 2022) reflected this past change in the prevailing forcing. Interestingly, the distribution of aerosol forcing itself (e.g., Oshima et al., 2020) was concentrated on the NH midlatitudes, but the pattern of relative precipitation response was quite different from that.

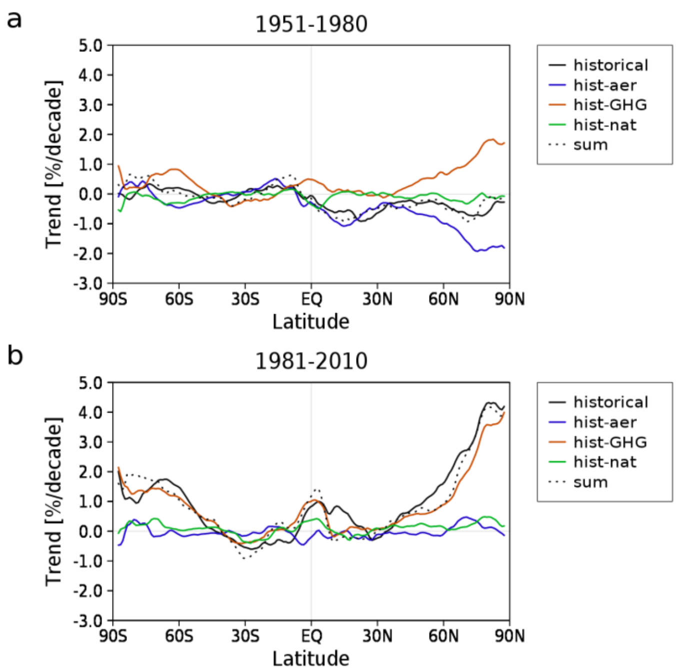

Figure 3. Meridional distributions of trends in zonal-mean relative precipitation changes for (a) Period I (1951–1980) and (b) Period II (1981–2010), shown for the historical (black), hist-aer (blue), hist-GHG (red), and hist-nat (green) experiments and the sum of hist-aer, hist-GHG, and hist-nat (dotted line). Values are trends in precipitation changes relative to the mean precipitation for 1850–1900 in historical simulation (in %/decade).

3.3 Constraining Factors for Past Precipitation Changes

From the DSE balance (Equation 1), precipitation changes were constrained by the atmospheric radiative cooling and the horizontal and vertical divergence of DSE. The precipitation trend over the Arctic region during Periods I and II was decomposed by these constraining factors (Figure 2b). In both periods (although the signs were opposite in different periods), radiative cooling and DSE horizontal divergence contributed to the precipitation trend with the same sign and similar magnitude. For example, the large increasing trend in precipitation in Period II was driven by enhanced radiative cooling of the atmosphere and a comparable increase in DSE horizontal divergence, corresponding to a decrease in heat transport from lower latitudes. The vertical divergence of DSE (i.e., the downward surface sensible heat flux) was in a direction that slightly moderated the horizontal divergence, although its magnitude was considerably smaller than those of the other components. The fractional composition by constraining factor was less dependent on the different forcing factors (Figure S3).

The enhanced radiative cooling in Period II was mainly dominated by clear-sky longwave radiative cooling, partially moderated by heating from clear-sky shortwave radiation, with little influence from cloud radiation (Figure S4). This can be attributed to the radiative responses to the higher temperatures and the associated increased water vapor (Pendergrass and Hartmann, 2014), although the contribution of water vapor change is generally small in the Arctic due to the very low absolute humidity. Bonan et al. (2023) decomposed changes in radiative cooling in response to warming into Planck feedback, temperature lapse-rate feedback, water vapor feedback, and albedo feedback. They argued that the polar amplification of relative precipitation change mainly results from Planck feedback. Planck feedback is an enhancement of radiative cooling for the vertical uniform temperature increase component, whereas temperature lapse-rate feedback, which reflects the vertical distribution of temperature change, considerably offsets the Planck feedback in the polar regions where the temperature increase is concentrated in the lower troposphere. We believe it is more appropriate to consider the combination of Planck feedback and temperature lapse-rate feedback as constraining factors for Arctic precipitation.

In Period I, the increase in shortwave heating worked toward decreasing precipitation, whereas the contribution of longwave radiation was a small negative (Figure S4a). Sulfate aerosol, the major component of the anthropogenic aerosol forcing that dominated in Period I, cooled the surface by scattering solar radiation, but its direct effect on radiative cooling of the atmosphere was considered negligible (Suzuki and Takemura, 2019; Oshima et al., 2020). The aerosol forcing included an increase in black carbon (BC), which absorbed shortwave radiation and heated the atmosphere directly. The increase in BC may contribute to reduced precipitation (Zhao and Suzuki, 2019; Oshima et al., 2020). However, isolating such effects from this analysis is difficult, and experiments with BC separate forcing would be needed.

Radiative cooling depends on the local conditions of the atmosphere (such as the air temperature), whereas DSE divergence depends on atmospheric circulation, including eddy activity and large-scale temperature structure (e.g., meridional temperature gradient). In summary, the rapid increase in Arctic precipitation in the recent past can be attributed to an enhancement of radiative cooling, which is a local effect of rising temperatures and a decrease in northward heat transport due to changes in the meridional temperature structure and eddy activity, both of which contributed in comparable magnitude to the rapid increase in precipitation in the Arctic region in the recent past.

3.4 Future Precipitation Changes and Constraining Factors

Figure 2c shows the recent past (Period II) and future (Periods III, IV, and V) precipitation changes in the Arctic region. Differences in future precipitation trends for the Arctic region between scenarios and time periods were qualitatively consistent with those in the Arctic temperature trends (Figure S5). In the near future (Period III), the trend of precipitation increase should remain almost the same regardless of the scenario (except for ssp585). In the medium to long term (Periods IV to V), precipitation increases are suppressed in the low-emission scenarios (ssp119, ssp126, and ssp245) as future temperature increases become smaller, whereas precipitation increases are enhanced in the high-emission scenarios (ssp370 and ssp585) as the temperature continues to rise.

The radiative cooling and the DSE divergence (the shading part and the rest of the bars in Figure 2c) contributed to the increase in precipitation in comparable magnitudes as constraining factors; the vertical divergent component of DSE (surface sensible heat flux) contributed very little in general (not shown). In the high-emission scenarios, the increase in DSE divergence was greater than the increase in radiative cooling at the end of the 21st century. This suggests that if warming is significant, changes in precipitation associated with changes in atmospheric meridional heat transport should be relatively more important. Because the radiative cooling component was nearly proportional to temperature change, the heat transport due to eddy activity may vary nonlinearly with respect to temperature change. However, the spread among models was greater for horizontal divergence than for radiative cooling, and uncertainty in heat transport changes was probably a major factor in the uncertainty of future precipitation changes.

3.5 Arctic Amplification of Precipitation Changes

The relationship between the Arctic amplifications of temperature and precipitation changes is discussed based on changes in various physical quantities in the historical experiment during Period II when GHG forcing was dominant (Figure 4). The temperature trend was larger at higher latitudes, reflecting the Arctic amplification of temperature changes (Figure 4a). The Arctic amplification factor as a ratio of the Arctic temperature trend to the global mean temperature trend was 2.7 in the CMIP6 multimodel mean. This value was within the range of previously reported values (Chylek et al., 2022). In contrast, the trend in relative precipitation (Figure 4b) was particularly large in the Arctic region—6.3 times larger than the global average. The apparent hydrological sensitivity obtained by dividing the relative precipitation trend by the temperature trend for each latitudinal band (Figure 4e) was about 3.7%/K in the Arctic region, which was more than twice the global, tropical, and midlatitude values. This means that the Arctic amplification of precipitation changes appears as a further doubling of the Arctic amplification of temperature changes.

From the above discussion, the following two pathways can be considered for Arctic amplification of precipitation changes.

(1) Larger temperature increases at higher latitudes lead to enhanced radiative cooling at higher latitudes (Figure 4f), leading to a larger precipitation increase in the Arctic.

(2) Reflecting the meridional gradient of temperature change (Figure 4d), the northward transport of DSE decreases, enhancing the horizontal divergence of DSE (Figure 4g), also leading to increased Arctic precipitation.

Considering (1) alone, the Arctic amplification of precipitation would be comparable to the Arctic amplification of temperature changes. However, the addition of (2) would further double the Arctic amplification of precipitation changes. As eddy activity primarily drives heat transport to the Arctic region, the connection with the meridional temperature gradient is not straightforward. However, Arctic amplification reduces the meridional temperature gradient (Figure 4d), which leads to a decreased northward DSE transport, even if there is no change in eddy activity. Note that the poleward transport of moist static energy (unlike DSE) increases as latent heat energy increases with warming (Hwang and Frierson, 2010; Audette et al., 2021).

Linear relationships exist between temperature change and precipitation change, including their constraining factor components (radiative cooling and horizontal and vertical DSE divergence), in the experiments with different forcings (Figure 2d). These relationships suggest that the above-mentioned mechanism does not depend on the type of forcing (i.e., aerosols, GHGs, or natural), as long as the temperature change is larger at higher latitudes. The proportion of each component's contribution is also less dependent on the forcing type.

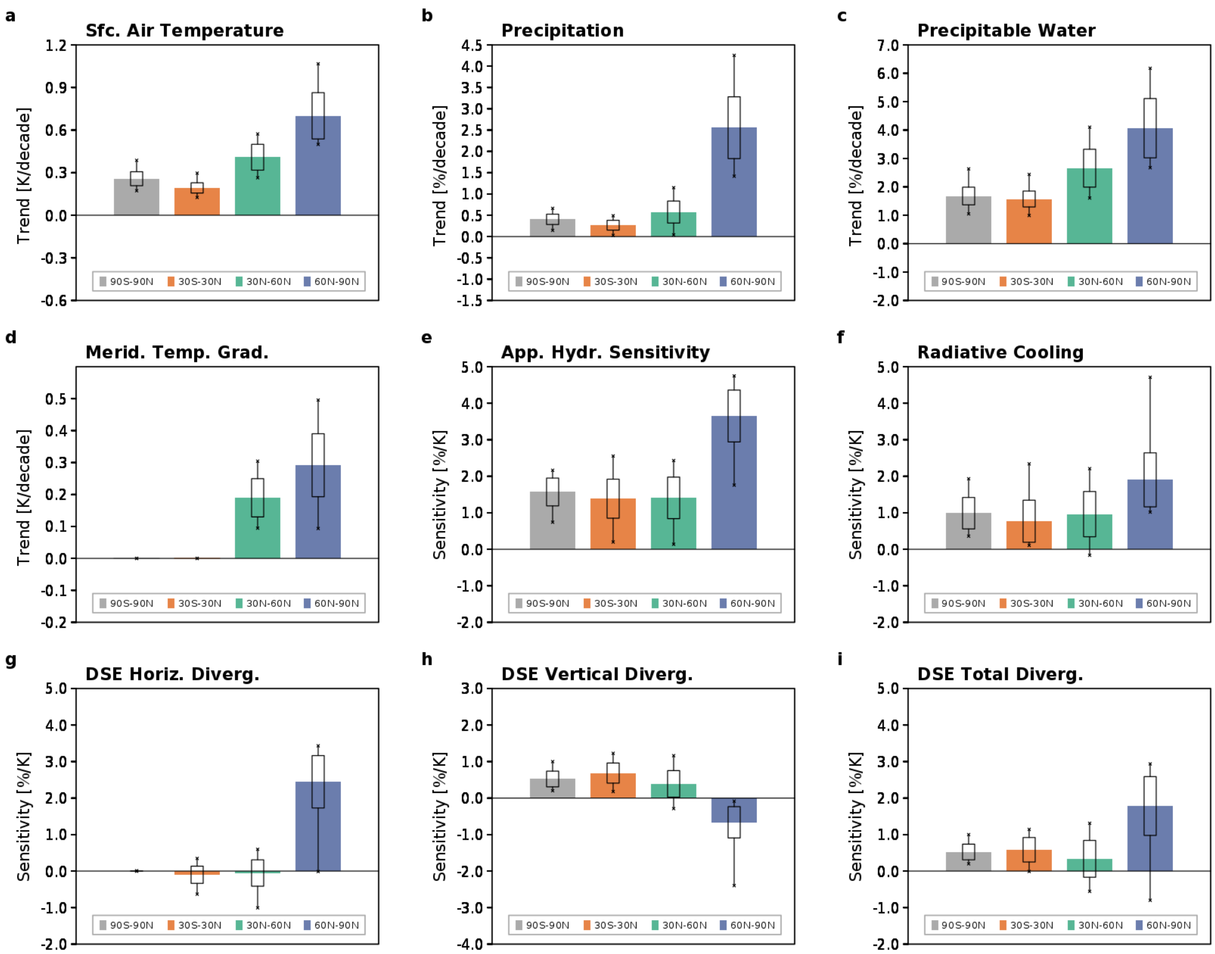

Figure 4. Apparent hydrological sensitivity by latitudinal zone and their constraining factors during Period II of the historical experiment. Trends in (a) surface air temperature (K/decade), (b) relative precipitation (%/decade), (c) column water vapor (precipitable water) (%/decade), and (d) meridional temperature gradient (K/decade) by latitudinal band. (e) Apparent hydrological sensitivity (%/K) and its breakdowns by constraining factors as (f) radiative cooling (%/K), (g) DSE horizontal divergence (%/K), (h) DSE vertical divergence (%/K), and (i) DSE total divergence (%/K). Bars are multimodel means; box–whisker plots represent the 30–70 percentile range of the intermodel spread and the maximum and minimum model values. The meridional temperature gradient is the difference between the mean temperature in the latitudinal bands of interest (30°N–60°N and 60°N–90°N) minus that in the southern latitudinal bands (0°N–30°N and 30°N–60°N).

4 Conclusions

CMIP6 multimodel historical and DAMIP experiments were analyzed to quantify the long-term changes in historical Arctic annual mean precipitation by forcing factor. In the recent past since the 1980s, aerosol forcing has been leveling off, whereas GHG forcing has continued to increase, resulting in a strong upward trend in Arctic precipitation. Based on the DSE balance, historical Arctic precipitation changes were decomposed by constraining factors. In addition to enhanced radiative cooling responding locally to increased air temperature being the dominant constraining factor for the trend of increased precipitation, enhanced DSE horizontal divergence (reduced heat transport from lower latitudes) associated with a larger temperature increase at higher latitudes (the Arctic amplification of temperature) was also a constraining factor with the same sign and comparable magnitude. The ScenarioMIP experiment results indicated that the relationship between precipitation change and temperature change in the future Arctic is similar to recent historical trends, with radiative cooling and DSE divergence contributing with similar magnitudes. The radiative cooling effect corresponding to local temperature changes, plus the effect of heat transport from lower latitudes reflecting the meridional gradient in temperature change associated with the Arctic amplification of temperature, results in a doubled Arctic amplification of precipitation changes relative to that of temperature changes.

Acknowledgments

This study was supported by the Environment Research and Technology Development Fund (JPMEERF20202003 and JPMEERF20232001) of the Environmental Restoration and Conservation Agency provided by the Ministry of the Environment of Japan, the Japan Society for the Promotion of Science (JSPS) KAKENHI (grant numbers: JP18H05292, JP19K03977, JP19H05699, JP21H03582, and JP23H00511), the Arctic Challenge for Sustainability II (ArCS II), Program Grant Number JPMXD1420318865, and a grant for the Global Environmental Research Coordination System from Ministry of the Environment of Japan (MLIT2253). The authors would like to thank Satoru Koizumi for his assistance in downloading, checking, and organizing the CMIP6 multimodel data for this analysis.

Open Research

All the used data from CMIP6 experiments (including the DAMIP and ScenarioMIP experiments) for models listed in Table S1 are available at the Earth System Grid Federation (ESGF) via the link https://esgf-node.llnl.gov/search/cmip6/. The observed HadCRUT5 temperature data were obtained from the link https://crudata.uea.ac.uk/cru/data/temperature/. The observed GPCP-SG precipitation data set accessed at http://eagle1.umd.edu/GPCP_CDR/Monthly_Data. The used ERA5 reanalysis data are available from the link https://doi.org/10.24381/cds.f17050d7.

References

Adler, R.F., M. Sapiano, & J.-J. Wang (2017). GPCP Version 2.3 SG Combined Precipitation Data Set. *NCEI CDR Program*, Asheville, NC. https://esgf.nccs.nasa.gov/esgdoc/GPCP_precip_SG-V2.3_TechNote_180510.pdf

Aizawa, T., Oshima, N., & Yukimoto, S. (2022). Contributions of anthropogenic aerosol forcing and multidecadal internal variability to mid-20th century Arctic cooling—CMIP6/DAMIP multimodel analysis. *Geophysical Research Letters*, 49(4), e2021GL097093. https://doi.org/10.1029/2021GL097093

Allen, M. R., & Ingram, W. J. (2002). Constraints on future changes in climate and the hydrologic cycle. *Nature*, 419(6903), 224-232. https://doi.org/10.1038/nature01092

Audette, A., Fajber, R. A., Kushner, P. J., Wu, Y., Peings, Y., Magnusdottir, G., ... & Sun, L. (2021). Opposite responses of the dry and moist eddy heat transport into the Arctic in the PAMIP experiments. *Geophysical Research Letters*, *48*(9), e2020GL089990. https://doi.org/10.1029/2020GL089990

Bengtsson, L., Hodges, K. I., Koumoutsaris, S., Zahn, M., & Keenlyside, N. (2011). The changing atmospheric water cycle in Polar Regions in a warmer climate. *Tellus* A: Dynamic Meteorology and Oceanography, 63(5), 907-920. https://doi.org/10.1111/j.1600-0870.2011.00534.x

Bintanja, R., & Selten, F. M. (2014). Future increases in Arctic precipitation linked to local evaporation and sea-ice retreat. *Nature*, *509*(7501), 479-482. https://doi.org/10.1038/nature13259

Bintanja, R., van der Wiel, K., Van der Linden, E. C., Reusen, J., Bogerd, L., Krikken, F., & Selten, F. M. (2020). Strong future increases in Arctic precipitation variability linked to poleward moisture transport. *Science advances*, *6*(7), eaax6869. https://doi.org/10.1126/sciadv.aax6869

Bonan, D. B., Feldl, N., Zelinka, M. D., & Hahn, L. C. (2023). Contributions to regional precipitation change and its polar-amplified pattern under warming. https://doi.org/10.1088/2752-5295/ace27a

Chylek, P., Folland, C., Klett, J. D., Wang, M., Hengartner, N., Lesins, G., & Dubey, M. K. (2022). Annual mean Arctic Amplification 1970–2020: Observed and simulated by CMIP6 climate models. *Geophysical Research Letters*, 49, e2022GL099371. htt https://doi.org/10.1029/2022GL099371ps://doi.org/10.1029/2022GL099371

Dagan, G., & Stier, P. (2020). Constraint on precipitation response to climate change by combination of atmospheric energy and water budgets. *npj Climate and Atmospheric Science*, *3*(1), 34. https://doi.org/10.1038/s41612-020-00137-8

England, M. R., Eisenman, I., Lutsko, N. J., & Wagner, T. J. W. (2021). The recent emergence of Arctic Amplification. *Geophysical Research Letters*, 48, e2021GL094086. https://doi.org/10.1029/2021GL094086

Gillett, N. P., Shiogama, H., Funke, B., Hegerl, G., Knutti, R., Matthes, K., ... & Tebaldi, C. (2016). The detection and attribution model intercomparison project (DAMIP v1. 0) contribution to CMIP6. *Geoscientific Model Development*, *9*(10), 3685-3697. https://doi.org/10.5194/gmd-9-3685-2016

Hersbach, H., Bell, B., Berrisford, P., Hirahara, S., Horányi, A., Muñoz-Sabater, J., ... & Thépaut, J. N. (2020). The ERA5 global reanalysis. *Quarterly Journal of the Royal Meteorological Society*, *146*(730), 1999-2049. https://doi.org/10.1002/qj.3803

Holland, M. M., & Bitz, C. M. (2003). Polar amplification of climate change in coupled models. *Climate dynamics*, *21*(3-4), 221-232. https://doi.org/10.1007/s00382-003-0332-6

Hwang, Y. T., & Frierson, D. M. (2010). Increasing atmospheric poleward energy transport with global warming. *Geophysical Research Letters*, *37*(24). https://doi.org/10.1029/2010GL045440

Manabe, S., & Wetherald, R. T. (1975). The effects of doubling the CO 2 concentration on the climate of a general circulation model. *Journal of Atmospheric Sciences*, *32*(1), 3-15. https://doi.org/10.1175/1520-0469(1975)032<0003:TEODTC>2.0.CO;2

McCrystall, M. R., Stroeve, J., Serreze, M., Forbes, B. C., & Screen, J. A. (2021). New climate models reveal faster and larger increases in Arctic precipitation than previously projected. *Nature Communications*, *12*(1), 6765. https://doi.org/10.1038/s41467-021-27031-y

Morice, C. P., Kennedy, J. J., Rayner, N. A., Winn, J. P., Hogan, E., Killick, R. E., ... & Simpson, I. R. (2021). An updated assessment of near-surface temperature change from 1850: the HadCRUT5 data set. *Journal of Geophysical Research: Atmospheres*, *126*(3), e2019JD032361. https://doi.org/10.1029/2019JD032361

Muller, C. J., & O'Gorman, P. A. (2011). An energetic perspective on the regional response of precipitation to climate change. *Nature Climate Change*, *1*(5), 266-271. https://doi.org/10.1038/nclimate1169

O'Neill, B. C., Tebaldi, C., Van Vuuren, D. P., Eyring, V., Friedlingstein, P., Hurtt, G., ... & Sanderson, B. M. (2016). The scenario model intercomparison project (ScenarioMIP) for CMIP6. *Geoscientific Model Development*, *9*(9), 3461-3482. https://doi.org/10.5194/gmd-9-3461-2016

Oshima, N., Yukimoto, S., Deushi, M., Koshiro, T., Kawai, H., Tanaka, T. Y., & Yoshida, K. (2020). Global and Arctic effective radiative forcing of anthropogenic gases and aerosols in MRI-ESM2.0. *Progress in Earth and Planetary Science*, *7*, 1-21. https://doi.org/10.1186/s40645-020-00348-w

Pendergrass, A. G., & Hartmann, D. L. (2014). The atmospheric energy constraint on global-mean precipitation change. *Journal of climate*, *27*(2), 757-768. https://doi.org/10.1175/JCLI-D-13-00163.1

Pithan, F., & Jung, T. (2021). Arctic amplification of precipitation changes—The energy hypothesis. *Geophysical Research Letters*, *48*(21), e2021GL094977. https://doi.org/10.1029/2021GL094977

Pithan, F., & Mauritsen, T. (2014). Arctic amplification dominated by temperature feedbacks in contemporary climate models. *Nature geoscience*, *7*(3), 181-184. https://doi.org/10.1038/ngeo2071

Previdi, M., Smith, K. L., & Polvani, L. M. (2021). Arctic amplification of climate change: a review of underlying mechanisms. *Environmental Research Letters*, *16*(9), 093003. https://doi.org/10.1088/1748-9326/ac1c29

Stjern, C. W., Lund, M. T., Samset, B. H., Myhre, G., Forster, P. M., Andrews, T., ... & Voulgarakis, A. (2019). Arctic amplification response to individual climate drivers. *Journal of Geophysical Research: Atmospheres*, *124*(13), 6698-6717. https://doi.org/10.1029/2018JD029726

Suzuki, K., & Takemura, T. (2019). Perturbations to global energy budget due to absorbing and scattering aerosols. *Journal of Geophysical Research: Atmospheres*, *124*(4), 2194-2209. https://doi.org/10.1029/2018JD029808

Yukimoto, S., Oshima, N., Kawai, H., Deushi, M., & Aizawa, T. (2022). Role of interhemispheric heat transport and global atmospheric cooling in multidecadal trends of northern hemisphere precipitation. *Geophysical Research Letters*, *49*(18), e2022GL100335. https://doi.org/10.1029/2022GL100335

Zhao, S., & Suzuki, K. (2019). Differing impacts of black carbon and sulfate aerosols on global precipitation and the ITCZ location via atmosphere and ocean energy perturbations. *Journal of Climate*, *32*(17), 5567-5582. https://doi.org/10.1175/JCLI-D-18-0616.1

Geophysical Research Letters

Supporting Information for

Factors Driving Past Trends in Arctic Precipitation and Their Future Changes

S. Yukimoto[1], N. Oshima[1], H. Kawai[1], M. Deushi[1], and T. Aizawa[1,2]

[1] Meteorological Research Institute, Japan Meteorological Agency, Tsukuba, Japan

[2] National Institute of Polar Research, Tachikawa, Japan

Contents of this file

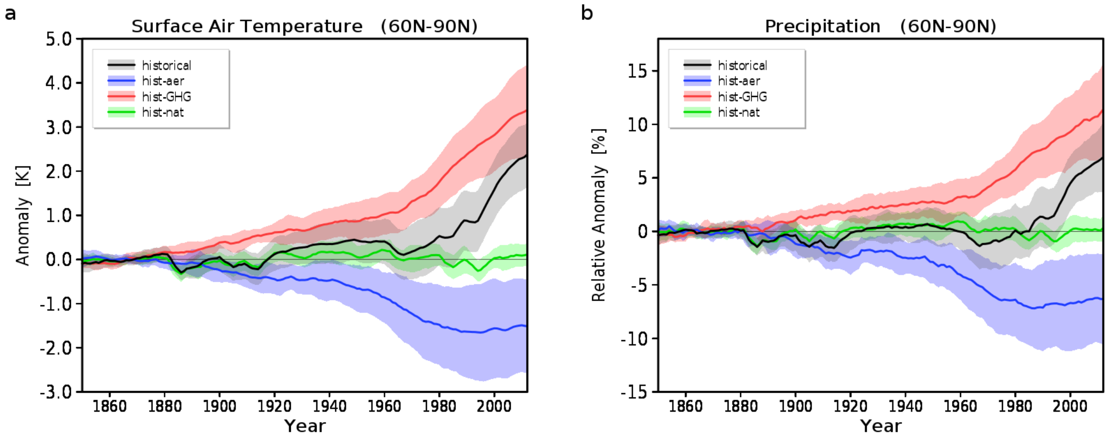

Figure S1. Time series of annual mean Arctic (60°N-90°N) (a) surface air temperature (K) and (b) relative precipitation (%) anomalies for the DAMIP experiments. Anomalies are relative to the 1851-1880 mean of the historical experiment. Colors indicate experiments by forcing; total forcing (historical, black), aerosol forcing (hist-aer, blue), GHG forcing (hist-GHG, red), and natural forcing (hist-nat, green). Solid lines indicate multi-model mean; shading indicates inter-model spread (30-70 %tile).

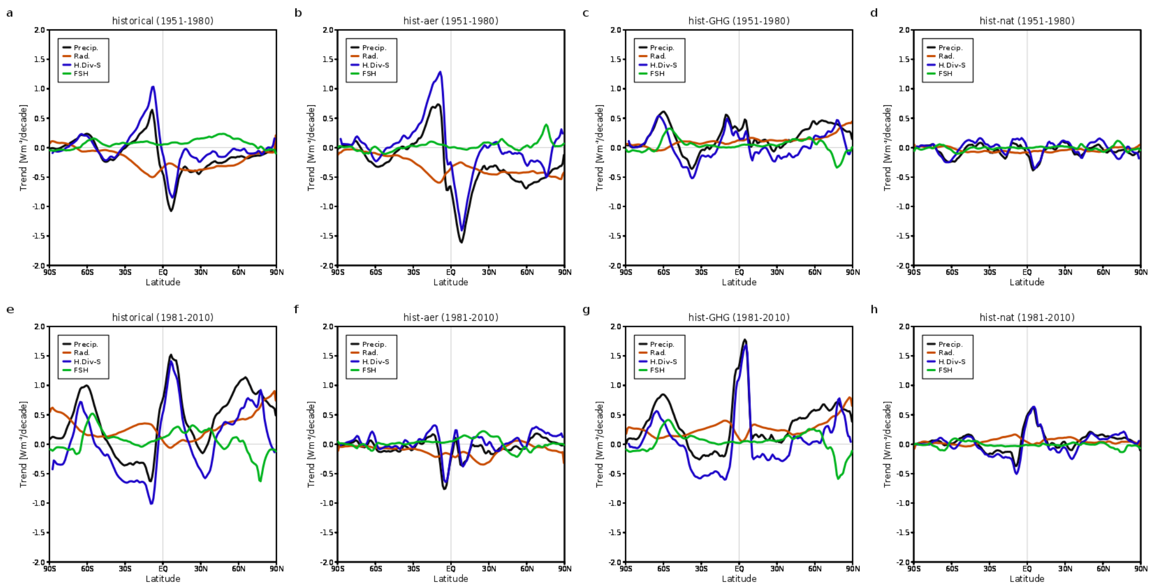

Figure S2. Meridional distributions of trends in zonal mean precipitation and their breakdown by constraining factors based on the (a, e) historical, (b, f) hist-aer, (c, g) hist-GHG, and (d,h) hist-nat experiments for (a-d) Period-I (1951-1980) and (e-h) Period-II (1981-2010). Colors indicate trend components of precipitation (black), radiative cooling (red), horizontal divergence of DSE (blue) and surface sensible flux (green).

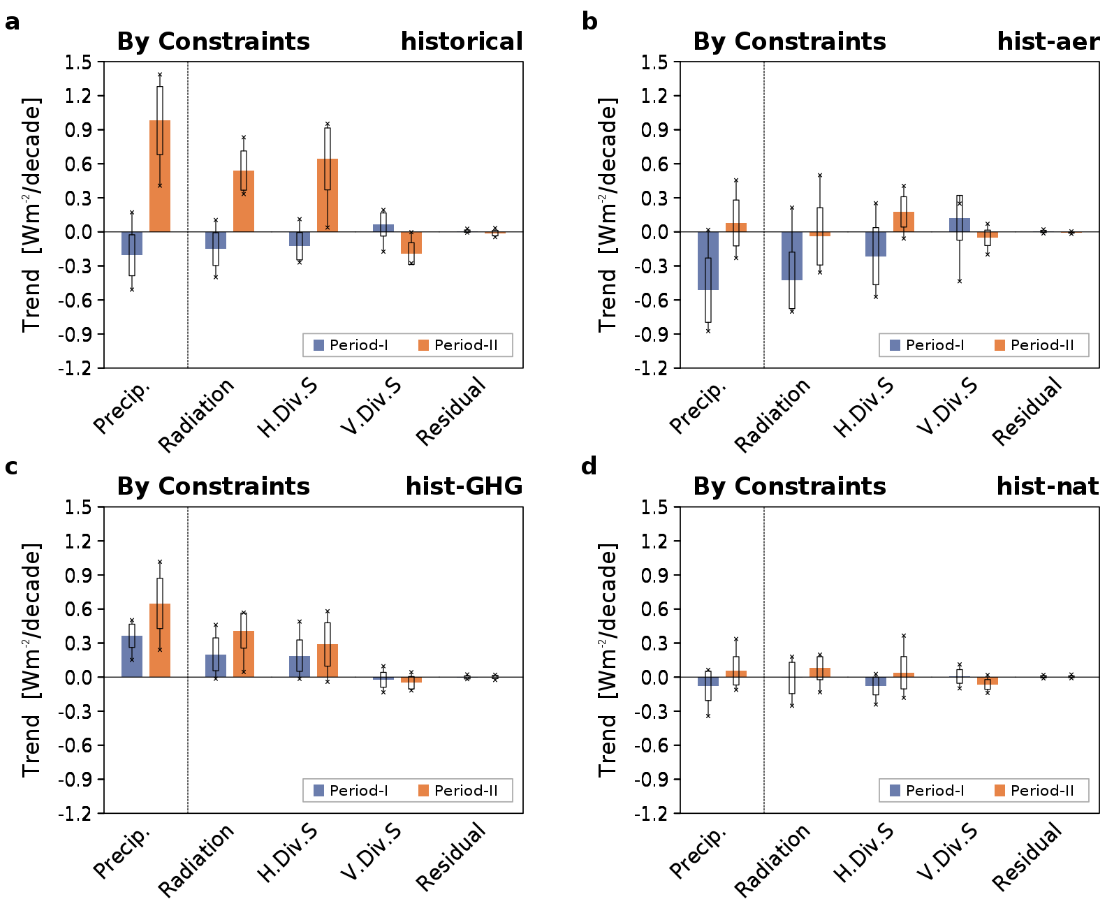

Figure S3. Arctic mean precipitation trend and its decomposition by constraining factors for the (a) historical, (b) hist-aer, (c) hist-GHG, and (d) hist-nat experiments. The precipitation trends (the leftmost of each panel) are decomposed into radiative cooling (Radiation), horizontal (H.Div.S) and vertical (V.Div.S) divergence of the DSE, and residual (Residual) components, for Period-I (blue) and Period-II (orange), respectively.

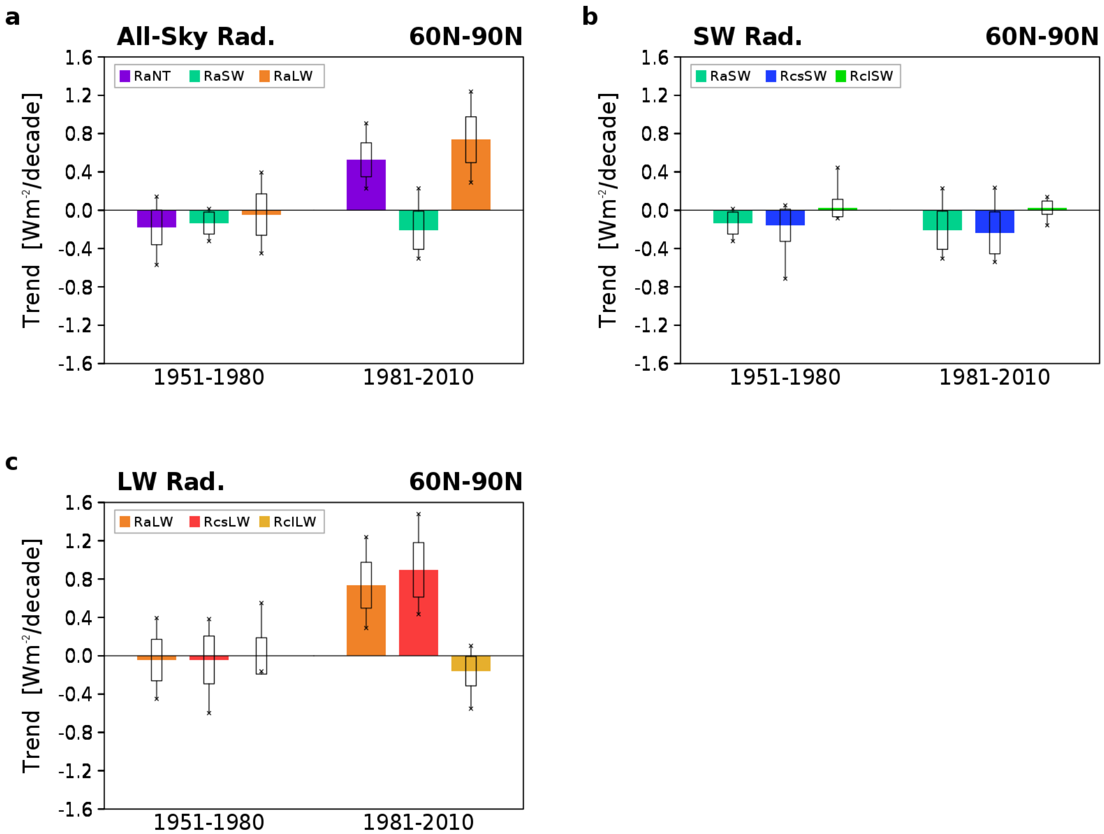

Figure S4. Radiative cooling components of the Arctic precipitation trends for (a) all-sky radiation, (b) shortwave radiation, and (c) longwave radiation. (a) Net (RaNT) and its breakdown into shortwave (RaSW) and longwave (RaLW) components, (b) all-sky shortwave (RaSW) and its breakdown into clear-sky (RcsSW) and cloud (RclSW) components, and (c) all-sky longwave (RaLW) and its breakdown by clear-sky (RcsLW) and cloud (RclLW) components. Each for Period I (1951-1980) and Period II (1981-2010) in the historical experiment.

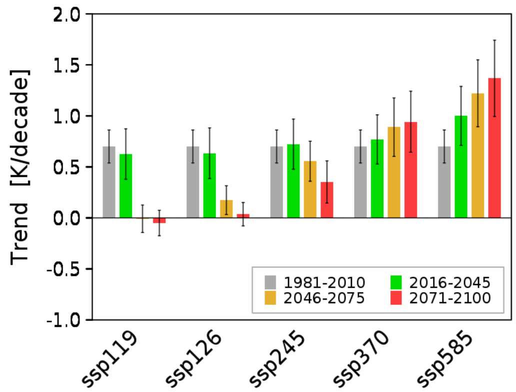

Figure S5. Present and future trends in Arctic mean surface air temperature, based on historical for Period II (1981-2010, gray), and each scenario experiment in ScenarioMIP (ssp119, ssp126, ssp245, ssp370, and ssp585) for Periods III (2016-2045, green), IV (2046-2075, yellow), and V (2071-2100, red).

Model	historical	hist-aer	hist-GHG	hist-nat	ssp119	ssp126	ssp245	ssp370	ssp585
ACCESS-CM2		3	3	3		5	5	5	5
ACCESS-ESM1-5	3	3	3	3		40	40	40	10
AWI-CM-1-1-MR								5	
BCC-CSM2-MR	3	3	3	3					
BCC-ESM1	3								
CAMS-CSM1-0	3								
CanESM5	50	30	50	50	50	50	50	50	50
CanESM5-CanOE						3	3	3	3
CESM2	11		3	3		3	3	3	3
CESM2-FV2	3								
CESM2-WACCM	3						5	3	5
CESM2-WACCM-FV2	3								
CNRM-CM6-1	30	10	10	10		6		6	6
CNRM-ESM2-1	9				5	5	10	5	5
E3SM-1-0	5								5
E3SM-1-1									
EC-Earth3	21				18	11	29	19	8
EC-Earth3-CC							9		
EC-Earth3-Veg	4				3	7	8	6	8
EC-Earth3-Veg-LR					3	3		3	3
FGOALS-f3-L	3								
FGOALS-g3	3	3	3	3		4	4	5	4
FIO-ESM-2-0						3	3		3
GFDL-CM4				3					
GFDL-ESM4				3					
GISS-E2-1-G	22	15	10	20	7	16	36	27	10
GISS-E2-1-H	12					10	10	6	10
GISS-E2-2-G						5	5	5	5
HadGEM3-GC31-LL	4	5	5	10			5		4
HadGEM3-GC31-MM									4
INM-CM5-0	10							5	
IPSL-CM6A-LR	32	10	10	10	6	6	11	11	7
KACE-1-0-G	3					3	3	3	3
MIROC6	10	10	50	50	50	50	50	50	50
MIROC-ES2L	3				10	10	30	10	10
MPI-ESM-1-2-HAM								3	
MPI-ESM1-2-HR	10							10	
MPI-ESM1-2-LR	10				30	30	30	30	10
MRI-ESM2-0	12	5	5	5	5	5	10	5	6
NESM3	5								
NorCPM1	30								
NorESM2-LM		3	3	3			13	3	
UKESM1-0-LL	17				5	16	17	16	5
Number of Models	30	12	13	15	12	22	24	27	26

Table S1. List of CMIP6 models used in the analysis for each experiment. Models in yellow cells are used for the analysis for the historical periods.